Exploring the impact of cooling rates and pressure on fragility and structural transformations in iron monatomic metallic glasses: Insights from molecular dynamics simulations

Soufiane Assouli, Hicham Jabraoui, Tarik El Hafi, Omar Bajjou, Abdelhadi Kotri, M'hammed Mazroui, Youssef Lachtioui

Highlights

Exploring the Impact of Cooling Rates and Pressure on Fragility and Structural Transformations in Iron Monatomic Metallic Glasses: Insights from Molecular Dynamics Simulations

Soufiane Assouli, Hicham Jabraoui, Tarik El hafi, Omar Bajjou, Abdelhadi Kotri, M'hammed Mazroui, Youssef Lachtioui

- Study explores Iron metallic glass under pressure (0-20 GPa) via MD simulations & cooling rates (5×10^{12}-10^{14} K/s).
- Increasing pressure impacts fragility, shown by higher activation energy. Cooling rates have relatively weak effects.
- Combined pressure & cooling rate influence on stability & atomic arrangement in iron metallic glasses observed.
- Higher pressure strengthens short-range order & progressive crystal nucleation, reflected in RDF peaks.
- Crystal-like clusters in bcc structure increase with all cooling rates, specific pressures cause distinct coordination changes.

Exploring the Impact of Cooling Rates and Pressure on Fragility and Structural Transformations in Iron Monatomic Metallic Glasses: Insights from Molecular Dynamics Simulations

Soufiane Assouli[a], Hicham Jabraoui[b,*], Tarik El hafi[a], Omar Bajjou[a], Abdelhadi Kotri[c], M'hammed Mazroui[d], Youssef Lachtioui[a]

[a]*Laboratory of Engineering in Chemistry and Physics of Matter Sultan Moulay Slimane University Faculty of Science and Technics of Beni Mellal BP. 523 23000 Beni Mellal Morocco.*
[b]*LAAS-CNRS University of Toulouse 31077 Toulouse France*
[c]*Physics Energy and Data Processing Laboratory Polydisciplinary Faculty of Ouarzazate Ibn Zohr University Ouarzazate Morocco*
[d]*Laboratory of Condensed Matter Physics University Hassan II Faculty of Sciences Ben MSik B.P. 7955 Casablanca Morocco*

Abstract

In this study, we investigate Fe metallic glass under pressures from 0 to 20 GPa and cooling rates of 5×10^{12} to 10^{14} K/s using molecular dynamics (MD) simulations with an embedded-atom potential (EAM). Increasing pressure enhances brittleness, indicating a higher barrier energy for the glass transition. Higher pressures narrow the glass transition region, resulting in a shorter relaxation range. At pressures above 10 GPa, especially with a cooling rate of 5×10^{12} K/s, crystal nucleation is promoted, and short-range order strengthens, primarily body-centered cubic structure (bcc) clusters. Certain pressure-cooling rate combinations show significant increments. Pressure affects density and interatomic distance, while cooling rate changes have minimal effects.

Keywords: Metallic glasses, Molecular dynamics, Fragility, Cooling rates, Pressure, Structural evolution

*Corresponding author
Email address: hicham.jabraoui@gmail.com, hicham.jabraoui@cnrs.fr (Hicham Jabraoui)

1. Introduction

Materials research aims to enhance the performance of structural materials for practical applications by tailoring specific microstructures. Among these fascinating engineering materials are metallic glasses (MGs) or vitreous solids, which gained attention in 1960 with the pioneering work of Klement and colleagues, who synthesized the first glassy alloy [1]. MGs, formed by rapidly quenching high-temperature melts, represent "frozen" liquids lacking long-range structural order [2]. Compared to their crystalline counterparts, most MGs exhibit improved mechanical, chemical, and magnetic properties due to the absence of structural defects like dislocations and grain boundaries [3, 4]. Among metallic glasses (MGs), Fe-based bulk glassy alloys stand out for their exceptional properties. They are particularly appealing due to their excellent soft magnetic characteristics, including a high saturation magnetization. Additionally, they exhibit remarkable electrical resistivity, exceptional mechanical strength, and cost-effectiveness, making them a compelling choice for various applications [5]. Their exceptional properties make MGs highly appealing for various applications, including aerospace, electronics, and biomedicine [6], where their unique combination of properties enhances performance and functionality [7, 8, 9].

Understanding the correlation between the structure and properties of glass materials, especially metallic glasses, is crucial in the field of material science. Numerous studies have investigated external factors, such as cooling rate and pressure, which have significant implications for the microstructure and properties of metallic glasses (MG) [10, 11, 12, 13]. For instance, higher cooling rates during solidification promote the development of homogeneous glassy structures, preventing the formation of regular crystalline arrangements and maintaining a non-crystalline, glassy state. Conversely, lower cooling rates permit atomic rearrangements, leading to the presence of crystalline regions within the material. Pressure also plays a significant role in shaping the microstructure and properties of metallic glasses, influencing atomic packing and bonding configurations.

Recent studies have employed molecular dynamics (MD) simulations to investigate the influence of cooling rates on the structural evolution and formation of metallic glasses [14], as well as the effects of pressure on monoatomic metallic glasses [15, 13]. In another investigation, researchers focused on a ternary bulk metallic alloy, namely the $Zr_{60}Cu_{20}Fe_{20}$ alloy, studying its atomic structures and the glass formation process using molecular dynamics simulations with many-body tight-binding potentials. The simulation results indicated that the $Zr_{60}Cu_{20}Fe_{20}$ alloy undergoes glass transformation when rapidly cooled to ap-

proximately 1000 K. Furthermore, the study emphasized the significant roles played by Cu and Fe atoms in the creation of an icosahedral environment within the alloy [16]. Another approach utilized X-ray diffraction and X-ray absorption fine structure, combined with reverse Monte Carlo (RMC) and ab initio molecular dynamics (AIMD) simulations, to investigate glass-based Fe materials [17]. The findings revealed that the addition of Y and Nb atoms to the binary Fe–B metallic glass primarily stabilizes large high-coordinated polyhedra by substituting the central Fe atoms, promoting the formation of icosahedron-like clusters and enhancing their connectivity with high-coordinated polyhedra [17].

To study the supercooling dynamics at the atomistic level, MD simulations have emerged as valuable tools due to the poor thermal stability of quenched liquids and the difficulty in directly measuring atomic movements and clusters. These simulations provide atomic-resolution information, aiding in correlating structural details with material properties and identifying contributing factors challenging to isolate in experiments [18, 19, 20, 21, 22]. Monoatomic metallic glasses offer unique opportunities for investigating glass formation and cluster development during rapid vitrification. In this study, we employ MD simulations to analyze the atomic-level structure of iron monocomponent MGs and understand microstructural growth during quenching under different pressures and cooling rates. Our choice of iron is based on its importance in multicomponent systems, where it has significant effects on microstructure and properties [23, 24].

We use various analytical techniques, including the Pair Distribution Function (PDF), Voronoi Tessellation Analysis (VTA), and Coordination Number Analysis (CNA), to investigate the structural evolution and the effects of pressure and cooling rate on atomic-level properties of monoatomic iron metallic glasses. Additionally, we quantitatively characterize the relationship between structure and glass transition temperature (T_g) to understand how increased pressure and cooling rate influence local structural changes in metallic glasses.

The article is structured as follows: Section 2 describes the system under investigation and the simulation methods used. In Section 3, we discuss in-depth the results obtained regarding the effects of cooling rate and pressure on the fragility and microstructural evolution of iron metallic glasses. Finally, we summarize our findings in the conclusion section.

2. Computational method

In this study, we investigated the behavior of Iron metallic glasses (MGs) using classical Molecular Dynamics (MD) simulations performed with the LAMMPS

(Large-scale Atomic/Molecular Massively Parallel Simulator) software [25]. The interactions between iron atoms were modeled using the embedded-atom method (EAM) potential parameterized by Zhou et al. [26]. This potential calculates the energy of each atom by considering its embedding in the local electron density of neighboring atoms in the Fe metal. The total energy of the system was computed using the equation:

$$E_{\text{tot}} = \sum_i F_i(\rho_i) + \frac{1}{2}\sum_{i \neq j} \Phi_{ij}(r_{ij}) \tag{1}$$

Here, Φ_{ij} represents the pair interaction energy between atoms i and j at a distance r_{ij}, while F_i denotes the embedding energy of an atom i in a local site characterized by an electron density ρ_i. The electron density ρ_i can be determined by:

$$\rho_i = \sum_{j, j \neq i} f_j(r_{ij}) \tag{2}$$

where $f_j(r_{ij})$ corresponds to the electron density at the location of an atom i, which arises from the presence of an atom j positioned at a distance of r_{ij}.

The initial MD simulations were performed in a cubic box with periodic boundary conditions in three directions, measuring 45.631 $\AA$ $\times$ 45.631 $\AA$ $\times$ 45.631 $\AA$. The system consisted of 8788 atoms organized in a lattice structure with a face-centered cubic (fcc) arrangement. A time step of 1 femtosecond (fs) was used, while the pressure and temperature were controlled using a Nose-Hoover barostat and a Nose-Hoover thermostat, respectively.

To achieve the glassy state of iron using MD simulations, we gradually heated the perfect crystal from 300 K to 3000 K at a heating rate of 1×10^{12} K/s in the NPT ensemble. This step allowed the initial structure to reach a fully liquid state at 3000 K, surpassing the melting point of iron (1811 K) and resulting in the loss of the system's structural memory. Subsequently, the system underwent a relaxation process for 100 picoseconds (ps) in the liquid phase under the Canonical NVT ensemble.

To investigate the impact of pressure on the formation of the glassy state, we applied pressures ranging from 0 to 20 GPa during the cooling process of the molten structure, gradually reducing its temperature from 3000 K to 300 K in the NPT ensemble. Various rapid cooling rates between 5×10^{12} and 1×10^{14} K/s were employed to achieve the glassy state of metallic iron. Finally, at room temperature, we ran a relaxation simulation at 300 K for subsequent data analysis. The visualization of atomic distributions and some examinations of atomic clusters

within the simulation box were carried out using the OVITO (Open Visualization Tool) package [27].

3. Results

In this section, we present the results of our investigation on the activation energy and fragility index, and their relationship with external parameters such as cooling rate and pressure. We also examine the influence of these external parameters on the microstructural properties of our simulated Fe system during the quenching process. To gain a comprehensive understanding of the microstructure details and identify key structural features, various analytical techniques have been employed.

3.1. Kinetic Properties

3.1.1. Glass Transition

Figure 1 illustrates the smooth variations in volume with temperature, showing two distinct slopes—one at low temperatures and another at high temperatures—each represented by separate fits. The intersection of these slopes marks the glass transition temperature (T_g), which distinguishes the transition from a liquid to a glass state. The glass transition is a fundamental concept in materials science and refers to the transformation of an amorphous material (glass) from a supercooled liquid state to a solid-like structure.

At higher cooling rates between $5 \times 10^{12}\,\mathrm{K/s}$ and $10^{14}\,\mathrm{K/s}$, the glass transition temperature (T_g) increases, indicating a notable rise (see Table 1). Rapid cooling prevents atoms from forming ordered crystalline structures, explaining this intriguing behavior. We established a critical point for the pressure-cooling rate relationship: at a cooling rate of $5 \times 10^{12}\,\mathrm{K/s}$ and a pressure of 10 GPa, the glassy state transition is absent. Instead, we observe an equilibrium liquid-crystallization transition (see Figure S1). Additionally, Figure 1 reveals a notable drop in volume occurring at a specific heating rate of ($10^{12}\,\mathrm{K/s}$), which indicates a transition from the liquid phase to a crystalline state. This abrupt change in volume is a consequence of the compact arrangement of atoms in the crystal phase compared to the more disordered liquid state.

Furthermore, Table 1 illustrates the influence of applied pressure on the glass transition process of iron, covering a range from 0 to $20,\mathrm{GPa}$. As pressure increases, the glass transition temperature rises, and simultaneously, the volume decreases. This behavior aligns with the concept that increased pressure densifies the material, reducing its free volume during the glass transition, which leads to

Table 1: Interatomic distance length, average coordination number (ACN), and density (ρ) of Fe-GM for different cooling rates. Each of these cooling rates has a different pressure applied in the range of 0 GPa to 20 GPa.

5×10^{12} K/s					
Pressure (GPa)	0	5	10	15	20
r (Å)	2.47	2.47	2.41	*xxx*	*xxx*
ACN	13.44	13.80	13.96	*xxx*	*xxx*
ρ (g/cm^3)	7.57	7.93	8.24	*xxx*	*xxx*
T_g (K)	1395	1664	*xxx*	*xxx*	*xxx*
10^{13} K/s					
Pressure (GPa)	0	5	10	15	20
r (Å)	2.47	2.47	2.41	2.41	2.40
ACN	13.44	13.60	13.76	13.75	13.96
ρ (g/cm^3)	7.58	7.87	8.12	8.35	8.60
T_g (K)	1474	1681	1771	1802	1880
5×10^{13} K/s					
Pressure (GPa)	0	5	10	15	20
r (Å)	2.47	2.47	2.47	2.41	2.41
ACN	13.42	13.58	13.45	13.69	13.79
ρ (g/cm^3)	7.56	7.85	8.11	8.33	8.52
T_g (K)	1509	1711	1780	1812	1883
10^{14} K/s					
Pressure (GPa)	0	5	10	15	20
r (Å)	2.47	2.47	2.41	2.41	2.41
ACN	13.41	13.56	13.71	13.70	13.79
ρ (g/cm^3)	7.55	7.85	8.10	8.32	8.53
T_g (K)	1544	1720	1794	1820	1890

r (Å)$\pm$0.01, ACN$\pm$0.05, ρ (g/cm^3)$\pm$0.01, T_g(K)$\pm$30

xxx means that in those cases we cannot estimate the glass state

enhanced atomic packing density [28]. Moreover, experimental investigations in $Zr_{65}Al_{7.5}Cu_{27.5}$ glass and $Pd_{40}Ni_{10}Cu_{30}P_{20}$ glass reveal intriguing results. In the case of $Pd_{40}Ni_{10}Cu_{30}P_{20}$ glass, with each 1 gigapascal (GPa) increase in pressure, the glass transition temperature (Tg) rises by 6 K. Conversely, in $Zr_{65}Al_{7\cdot5}Cu_{27.5}$ glass, researchers observed that with every 5 GPa increase in pressure, the T_g increases by 50 K [29].These findings emphasize the central role of pressure in increasing viscosity and transitioning to a glassy state at high temperatures, with the caveat that the glass transition temperature (T_g) must be lower than the melting temperature (T_m) for this process to proceed smoothly. However, under certain conditions combining high pressures and low cooling rates, pressure not only increases the viscosity but also hinders the formation of free volumes. The low cooling rate allows the system to relax over a long time, and applying pressure to the system helps the supercooled liquid crystallize under pressure[29]. At high pressure and low cooling rates, rather than undergoing a glass transition, the material solidifies at a higher temperature where (T_g) could equal (T_m). When examining the volume–temperature relationship, we observe an equilibrium-like transition from a pure liquid to a solid, crystalline state (see Figure S1 in the Supporting Material file). Previously reported work [30] noted that due to the large increase in the viscosity of an Fe melt under compression, rapid cooling (10^3–10^6 K/s) of the melt under pressures $P \leq 0.5$–1 Mbar should lead to solidification into a nanocrystalline state.

3.1.2. Activation energy and fragility index determination

In a previous study, Ritland proposed an equation [31, 32, 33] that originally related the cooling rate and fictive temperature for glasses without memory. Here, T_f is obtained as the glass is cooled through the transition region [34, 10, 35]. In our present study, we have extended this equation to cover glasses with memory, characterized by a range of relaxation times. The main aim of this investigation is to establish a correlation between the cooling rate (b) and T_g, which shares a similar concept with T_f.

Interestingly, when the spectrum of relaxation times is temperature-independent, the glass transition temperature (T_g) achieved during the rapid cooling of a supercooled liquid (in a viscous state) to a glass state (in a frozen state) is found to be related to the cooling rate (b) in the following manner:

$$-\frac{d\ln(b_c)}{d\left(\frac{1}{T_g}\right)} = \frac{-\Delta h^*}{R} \tag{3}$$

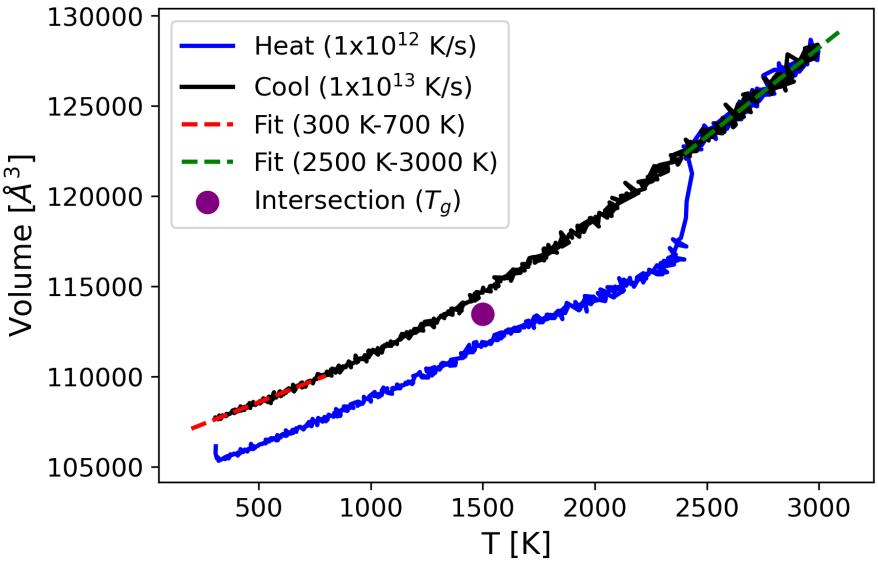

Figure 1: A representative case illustrating the determination of the glass transition temperature (T_g) of iron (Fe) using the fitting method. Heating and cooling rates were 10^{12} K/s and 10^{13} K/s, respectively, at 0 GPa. This method was applied to determine T_g for all cooling rates and pressures. The intersection between the low-temperature and high-temperature regions indicates T_g. Note: An equilibrium liquid-crystallization transition observed during heating.

where R represents the universal gas constant, and Δh^* corresponds to the energy governing molecular mobility and atomic rearrangement around the glass transition temperature T_g. Figure SM2 illustrates an Arrhenius plot, depicting the correlation between the logarithm of the cooling rate and the glass transition temperature for Fe-MGs. Various pressures applied during the glass transition process are considered within each cooling rate range.

Table 2 reveals a significant relationship between pressure and the activation enthalpy of relaxation time during the Fe-MGs glass transition process. Increasing pressure leads to a rise in activation energy from 364.34 kJ/mol at 0 GPa to 6120 kJ/mol at 20 GPa. This demonstrates that applying pressure to Fe-MGs creates additional resistance, hindering the material's ability to overcome the kinetic barrier associated with the glass transition. The mobility of atoms and molecules in the material is affected by pressure during the glass transition, with higher pressure making it more challenging for the necessary atomic rearrangements to occur. The increased packing of atoms under pressure results in stronger interatomic forces, limiting their movement and elevating the activation energy re-

quired to surmount these barriers. In a related context, Scott [36] employed differential scanning calorimetry (DSC) to study the crystallization kinetics of two Fe-Ni metallic glasses near their glass transition temperature. The analysis of the time required to reach 50% transformation allowed estimation of the activation energies for crystallization, which were found to be around 418 kJ/mol. Furthermore, pressure has an impact on the thermodynamic stability of the glassy state. With increasing pressure, the glass transition temperature (T_g) shifts to higher values. This implies that achieving the glassy state requires cooling the supercooled liquid above T_g, thereby increasing the barrier energy. The increased pressure also raises the viscosity of the supercooled liquid, leading to slower molecular motion and greater resistance to flow. Consequently, this contributes to a higher energy barrier for the glass transition. Additionally, under higher pressure, the atomic structure of the material becomes more rigid and less amenable to forming the disordered structure characteristic of the glassy state. Under extremely high pressures, the situation becomes more complex. The pressure not only increases viscosity but also impedes the formation of free volumes. In these unique conditions characterized by high pressure and low cooling rates, it's possible for the glass transition temperature (T_g) to align closely with the melting temperature (T_m). This alignment results in a more stable configuration, especially at lower cooling rates, providing ample time for relaxation, which can ultimately lead to crystallization. In scenarios of high pressure coupled with low cooling rates, rather than experiencing a traditional glass transition, we observe a distinctive equilibrium-like transition from a pure liquid to a solid, crystalline state (see Figure S1 in the Supporting Material file).

Table 2: The glass transition activation enthalpy Δh^* of monatomic Fe-MGs.

Pressure (GPa)	0	5	10	15	20
Δh^* (kJ/mol)	364.34	1263.41	2532.70	3525.88	6120.44
$\delta \pm$ (kJ/mol)	11.37	10.35	110.22	67.98	357.03

The fragility of Fe-MGs, considering its response to different pressure conditions, can be calculated based on the obtained activation enthalpy results, Δh^*. This calculation allows for the quantification of the material's fragility, which is a measure of its susceptibility to undergo structural changes near the glass transition region. This fragility, denoted as "m", can be determined using the following formula [37, 38]:

$$m = \frac{\Delta h^*}{\ln(10) R T_g} \tag{4}$$

The fragility index of the glass can be determined using an alternative approach based on the determination of the glass transition range ($T_{g(end)} - T_g$) [37, 38], leading to a second definition of 'm' as follows:

$$m = \frac{2.1 T_g}{T_{g(end)} - T_g} \tag{5}$$

The fragility index is a measure of how quickly a material undergoes structural changes near T_g (glass transition temperature). It quantifies the temperature dependence of the relaxation time in the glassy state. In summary, the increase in the fragility index with pressure indicates that higher pressure hinders the structural rearrangement and relaxation processes, making the Fe material more prone to undergoing rapid structural changes near the glass transition temperature. The increase in the fragility index with increasing pressure results in a transition from a strong-to-fragile behavior. This behavior aligns with findings reported for glass-forming liquids in previous studies [39, 40]. However, it's worth noting that some other research has suggested a pressure-induced increase in the fragility of glassy materials [41, 42].

The relatively limited range of the parameter 'm' in our simulations may be attributed to the lower cooling rate used compared to the experimental conditions employed for determining T_g. However, we maintain confidence in the accuracy of our estimated T_g value, and as a result, we employ it to characterize the fragility of the liquid in our study. It is worth noting that a narrower range of fragility index has been observed in a prior investigation [40]. Conversely, it is well-documented that the presence of multiple components in alloys generally leads to a decrease in the kinetic fragility of metallic glass-forming liquids [43, 44, 45]. Therefore, it is reasonable to assume that the fragility of pure metals would be considerably higher than that of multicomponent alloys. Furthermore, considering the relationship between fragility and thermodynamic properties, achieving such a low 'm' value would necessitate a significantly small difference in heat capacity at T_g, which requires further substantiation [46].

By equating the two expressions for the fragility index, the temperature range ($T_{g(end)} - T_g$) can be determined as:

$$T_{g(end)} - T_g = \frac{2.1 T_g}{\frac{\Delta h^*}{\ln(10) R T_g}} \tag{6}$$

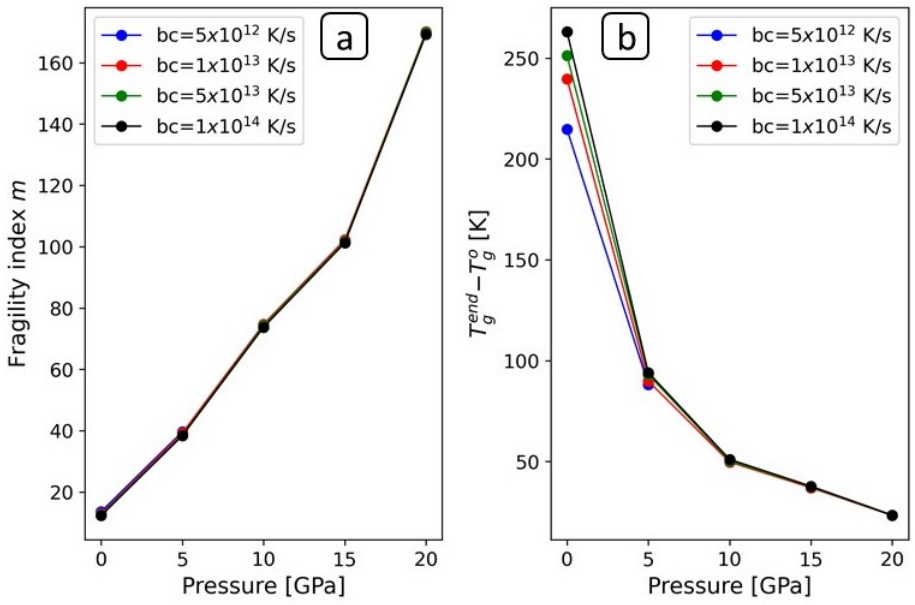

Figure 2: (a) Fragility index m variation and (b) relaxation temperature $(T_g^e - T_g^o)$ for a glass forming under different cooling rates: 5×10^{12} K/s, 1×10^{13} K/s, 5×10^{13} K/s, and 1×10^{14} K/s, as a function of pressure in Fe-MGs.

Figure 2b presents interesting information about the behavior of the glass transition region $(T_{g(end)} - T_g)$ under different pressure conditions. It is evident that when the pressure decreases, the glass transition region widens, while it narrows when the pressure increases. This significant variation in the width of the glass transition region suggests the presence of various structural configurations for the Fe MGs.

At lower pressures, the temperature range exhibiting a broad glass transition region indicates the existence of multiple events and structural configurations with relatively low barrier energy for crossings. In other words, under low pressure, the metallic glass experiences a wider temperature range over which it undergoes transitions between different structural states, and these transitions occur more easily due to the reduced energy barriers. The larger glass transition region observed under low-pressure conditions suggests that the MG-Fe system is more sensitive to structural rearrangements, resulting in a greater degree of configurational diversity. These different structural configurations can coexist and play a crucial role in determining the properties and behavior of the material.

On the other hand, as the pressure increases, the glass transition region narrows, indicating that the MG-Fe system becomes more constrained with small

free volumes and exhibits fewer structural changes in a smaller temperature range. This suggests that higher pressures stabilize the structure, limiting the number of configurations available and making transitions between them less likely.

3.2. Structural properties

3.2.1. Pair distribution function

The pair distribution function (PDF) analysis is one of the most important approaches for revealing the structural properties of a model system, especially for crystal, liquid, and glass systems. The PDF, denoted as $g(r)$, provides information about the probability of finding an atom at a distance r from a central atom in the system. In a system consisting of a single type of atom, the PDF can be expressed as [47]:

$$g(r_i) = \frac{V}{N^2} \left\langle \sum_{j \neq i}^{N} \frac{n(r_i)}{4\pi r_i^2 \Delta r_i} \right\rangle. \tag{7}$$

Here, V represents the total volume of the simulation system, N is the number of atoms, and $n(r)$ denotes the number of atoms located at a distance r from the central atom within the shell $[\Delta r, \Delta r + dr]$. Figure 3 presents the PDF curves for Fe-MGs at 300 K, obtained by varying pressures and cooling rates. PDF curves represent atomic correlations and can provide insights into the local atomic structure. The first peak in any curve indicates the interatomic distance between the central atom and its closest first neighbors, as indicated in Table 1. An advantage of the pair distribution function (PDF) is that the presence of two clustering peaks in monatomic metallic glasses as a second peak can be a signature of the formation of the glass system.

Figure 3 presents the PDF curves for Fe-MGs at 300 K, obtained by varying pressures and cooling rates. Figure 3(a) corresponds to a cooling rate of 5×10^{12} K/s with a pressure range applied from 0 to 20 GPa. Notably, as the pressure increases, around 5 GPa, a distinct shoulder begins to form on the right side of the first maximum peaks, accompanied by a splitting at the second peak of the PDF curves at approximately 4.7 Å. These shoulders become more prominent with increasing pressure. This suggests that at a low cooling rate (resulting in a long transition time), the presence of crystalline clusters in the system becomes evident, especially as the pressure reaches extremely high levels. When molten iron is cooled under 10^{13} K/s and the pressure gradually increases from 0 to 15 GPa (Figure 3(b)), a splitting at the second peak of the PDF curve and a shoulder between the first and second peaks of the PDF begin to appear as pressure

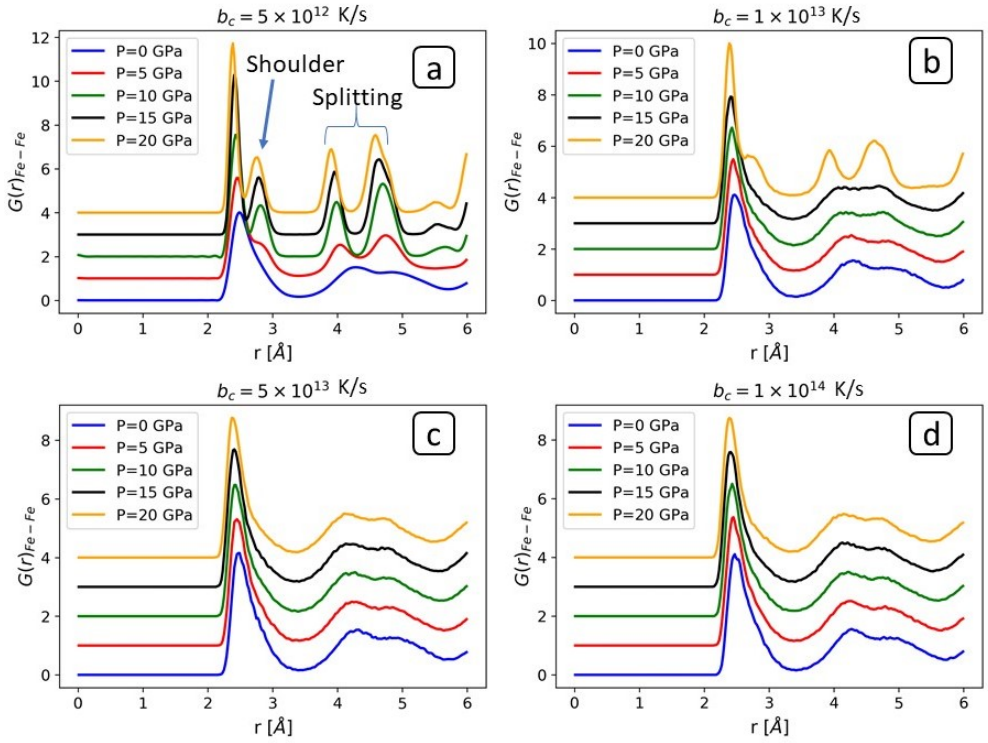

Figure 3: RDFs for monatomic iron at 300 K under various quenching conditions of pressure: (a) for the cooling rate of 5×10^{12}, (b) for the cooling rate of 1×10^{13}, (c) for the cooling rate of 5×10^{13}, (d) for the cooling rate of 1×10^{14}. Note that the first peak represents the interatomic distance between the central atom and its neighbors, and the distinct splitting of a broad second peak and the appearance of a shoulder close to the second peak is a signature of crystalline formation.

increases. In this case of cooling rate, the shoulders become noticeable only at a very high pressure of approximately 20 GPa, at which point the system forms a crystalline state. Figure 3(c) and Figure 3(d) exhibit similar behavior, representing even higher cooling rates of 5×10^{13} K/s and 10^{14} K/s, respectively, while maintaining the same pressure range. In both cases, the appearance of noticeable shoulders is observed beyond the 20 GPa threshold. The appearance of a shoulder just after the first peak and the distinct splitting of the second broad peak can be considered as a signature of crystallization in the system under certain conditions during the cooling process, namely pressure and cooling rate. In conclusion, with a very rapid cooling rate, in our case, 5×10^{13} and 1×10^{14}, there is no crystallization within the entire range of pressure, from 0 GPa to 20 GPa. In the case of 1×10^{13}, crystallization occurs starting from 20 GPa, and in the case of 5×10^{12},

it begins at around 5 GPa. The low cooling rate allows the system to relax over a long time, and applying pressure to the system helps supercooled liquid crystallize under pressure[29].

3.2.2. Voronoi tessellation analysis and coordination number

In order to gain a more comprehensive understanding of the microstructure at a local level in liquids and amorphous solids, the Voronoi polyhedron (VP) approach was introduced by Finney [48]. This template-free technique involves partitioning three-dimensional space into polyhedra centered around individual atoms. The polyhedra consist primarily of triangles, quadrilaterals, pentagons, and hexagons. The local structures of these polyhedra can be characterized using Voronoi indices denoted as $< n_3, n_4, n_5, n_6 >$, where n_i represents the number of i-edged faces in the VP. The Voronoi indices also serve as a measure of the total coordination number CN $= \sum_i n_i$, allowing for differentiation and classification of the type of polyhedron surrounding a central atom within a specified cutoff distance[49]. Hwang et al.[50] further categorized the various forms of VP into three distinct groups: crystal-like clusters ($< 0,4,4,x >$), mixed-like clusters ($< 0,3,7,x >$ and $< 0,3,6,x >$), and icosahedral-like clusters ($< 0,1,10,x >$, $< 0,2,8,x >$, and $< 0,0,12,x >$), where x typically assumes values within the range of 0 to 6.

Figure 4 illustrates the variation of the percentages of the top five most populated VPs in Fe-MGs as a function of pressure at different cooling rates. The VPs considered are $< 0,0,12,0 >$, $< 0,1,10,2 >$, $< 0,2,8,4 >$, $< 0,4,4,6 >$, and $< 0,6,0,8 >$. The results indicate that only the $< 0,4,4,6 >$ polyhedron, which represents crystal-like clusters, and the $< 0,6,0,8 >$ polyhedron, which corresponds to a body-centered cubic structure (bcc), both show a significant increase in their percentages across all quenching rates. This increase becomes particularly pronounced when a specific pressure value corresponding to the given cooling rate is applied. Therefore, there is a specific pressure-cooling rate combination that triggers a notable increase in the percentages of these two polyhedrons. As the cooling rate is further increased, the pressure required for this substantial increase also takes on greater values. This trend is clearly illustrated in Figure 4(a) and Figure 4(a) for cooling rates of $5 \times 10^{12}\,\mathrm{K/s}$ and $10^{13}\,\mathrm{K/s}$, respectively. In these cases, the significant increase happens at approximately 5 GPa and 20 GPa, respectively. For cooling rates higher than the ones previously discussed (see Figure 4(c-d)), the substantial increase in the percentages of the $< 0,4,4,6 >$ and $< 0,6,0,8 >$ polyhedrons occurs at pressure values exceeding 20 GPa as indicated in Figure SM5. Conversely, the remaining polyhedra, $< 0,0,12,0 >$,

$< 0,1,10,2 >$, and $< 0,2,8,4 >$, which constitute icosahedral-like clusters, exhibit a decrease in their percentages as pressure increases from 0 to 20 GPa for a high cooling rate. This trend continues even at pressures beyond 20 GPa. This implies that the atomic arrangement associated with these polyhedra becomes energetically less favorable under these conditions, suggesting a tendency toward a more crystalline state within the system. Taking into account the effect of cooling rate, Figure S6 presents the variation in the percentages of the top five most populated Voronoi polyhedra (VPs) in Fe-MGs at 0 GPa under different cooling rates. Here, we find that there are no specific trends; each unit presents fluctuated values within a range of cooling rates, which is consistent with a previous study on Ni monoatomic glass[14].

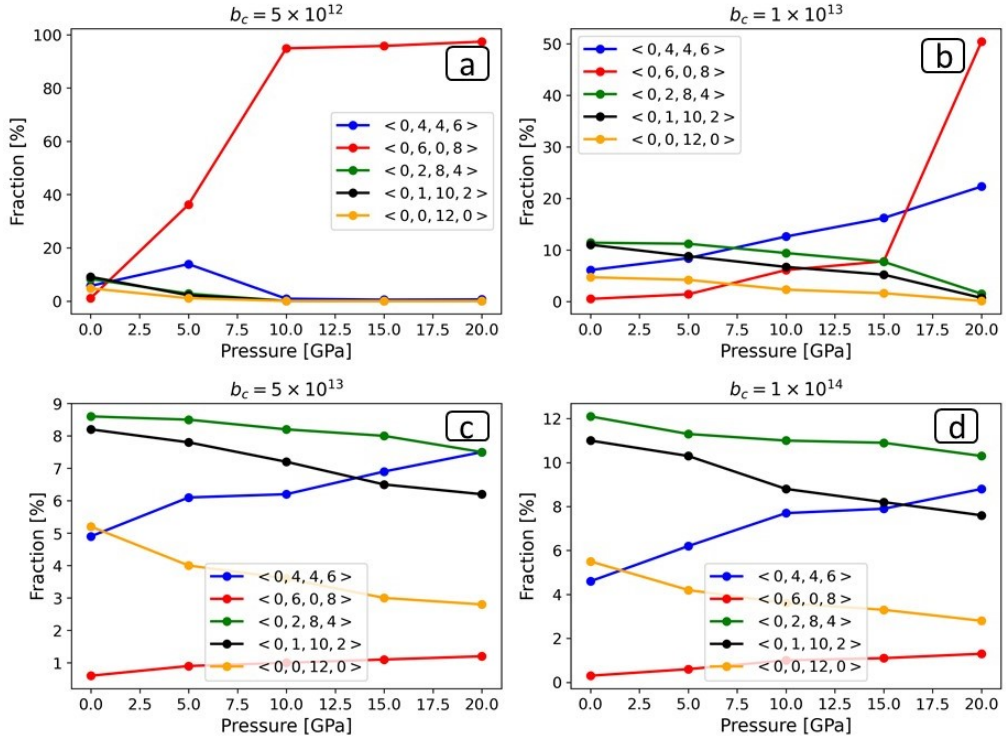

Figure 4: Pressure-dependent variation of the most populated Voronoi polyhedra fractions in Fe-MGs formed at 300 K under various quenching conditions of pressure: (a) for the cooling rate of 5×10^{12} K/s, (b) for the cooling rate of 1×10^{13} K/s, (c) for the cooling rate of 5×10^{13} K/s, (d) for the cooling rate of 1×10^{14} K/s.

Figure SM3 showcases the development of the bcc structure and crystal-like clusters within the iron system at room temperature while varying the pressure and

quenching rates. The figure clearly illustrates the significant influence exerted by both pressure and cooling rate on the formation and evolution of microstructures. It becomes apparent that, despite the fact that a higher cooling rate promotes the iron vitreous state, there exists a specific pressure value that can induce a structural transition from an amorphous-like state to a more crystalline structure within the system. These findings align well with the previous results reported in Figure 4.

The distribution of coordination numbers (CNs), which reflects the number of atoms bonded to a reference atom in its nearest neighbor shell, is another way to analyze the structure of our investigated system. In the subsequent discussion, we will focus on the pressure-dependent changes in the different CNs under various quenching rates. Figure 5 illustrates the distribution of CNs in Fe-MGs at the end of the quenching process using four different cooling rates and pressures varying from 0 to 20 GPa. The analysis reveals that $> 98\%$ of the atoms in the Fe system possess CNs between 12 and 16. Furthermore, it demonstrates that as the cooling rate increases, a broader distribution of CNs is observed. This means that the system exhibits a wider range of coordination numbers beyond CN=14, including CN=12, CN=13, CN=15, and CN=16. However, with the application of pressure applied to the glass transition process, especially at certain values, there is a distinct rise in the fraction of atoms with a coordination number of CN=14, resulting in a decrease in the fraction of atoms with other CNs. This signifies that the atoms in the Fe molten system tend to arrange themselves in a structure where each atom is surrounded by approximately 14 neighboring atoms. For instance, in Figs. 7(a) and 7(b) representing cooling rates $5 \times 10^{12}\,\mathrm{K/s}$ and $10^{13}\,\mathrm{K/s}$, respectively, a significant increase in the coordination number CN=14 is observed at pressure values of 5 GPa and 20 GPa. Similarly, for higher cooling rates of $5 \times 10^{13}\,\mathrm{K/s}$ and $10^{14}\,\mathrm{K/s}$ depicted in Figure 5c and Figure 5d, respectively, a higher pressure exceeding 20 GPa is required to observe the same behavior. This implies that as the cooling rate becomes faster, a higher pressure is necessary to induce a large fraction of CN=14. These findings highlight the interplay between pressure applied upon the glass transition process and cooling rate in shaping the distribution of CNs in Fe-MGs. Increasing pressure promotes the rise of CN=14, reflecting denser atomic packing. Conversely, higher cooling rates result in a broader distribution of CNs, suggesting a more varied and disordered atomic arrangement.

For a closer examination of the coordination distributions in the simulated iron system, Figure 6 displays three-dimensional configurations under various conditions employed in the quenching process. The atoms are color-coded according to their CN. Regardless of the cooling rate, the system is disordered in a vacuum environment. Indeed, the development of a crystalline structure with 14 neighbors

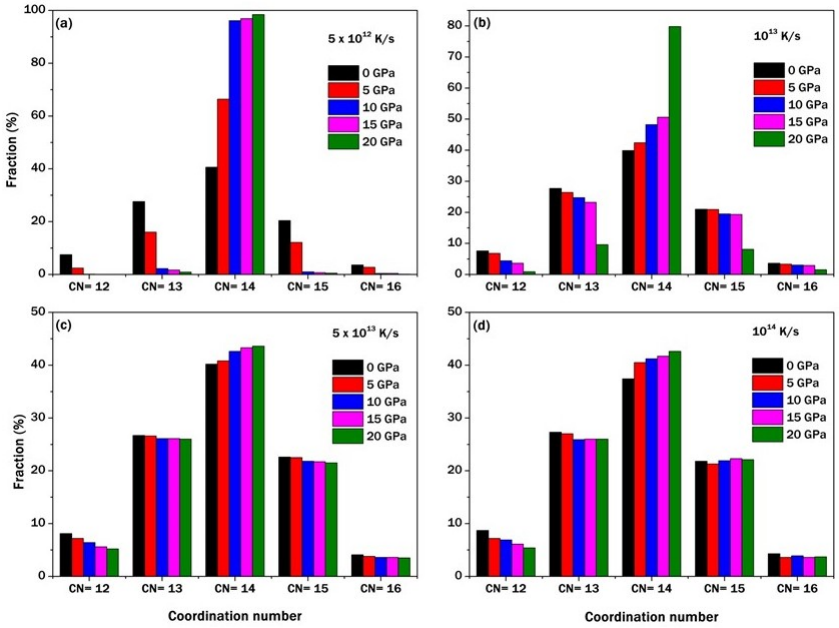

Figure 5: Histogram presenting the percentage of coordination numbers of glassy iron atoms prepared under different quenching conditions, namely cooling rates in the range of 5×10^{12}-1×10^{14} and pressures in the range from 0 to 20 GPa.

(CN=14) is clearly visible by the increase in pressure.

We note that the visual representations corresponding to the effects of the other values of cooling rates and pressures on the formation and evolution of microstructures (see Figure SM3) and coordination number distribution (see Figure 5 and Figure 6) are not included here, as they yielded similar behaviors and conclusions. Figure 7 provides visual depictions of the predominant Voronoi polyhedra. These snapshots illustrate that certain clusters possess the same coordination numbers, but their rotational symmetries and geometric structures differ.

4. Discussion

The results of this study provide valuable insights into the influence of applied pressure on the glass transition process and cooling rate on the brittleness and structural evolution of Fe-MG. The observed increase in activation energy with higher pressure indicates that elevated pressures make the glass transition process more difficult and energetically demanding. Consequently, the material exhibits higher fragility, becoming more sensitive to variations in pressure. On the other

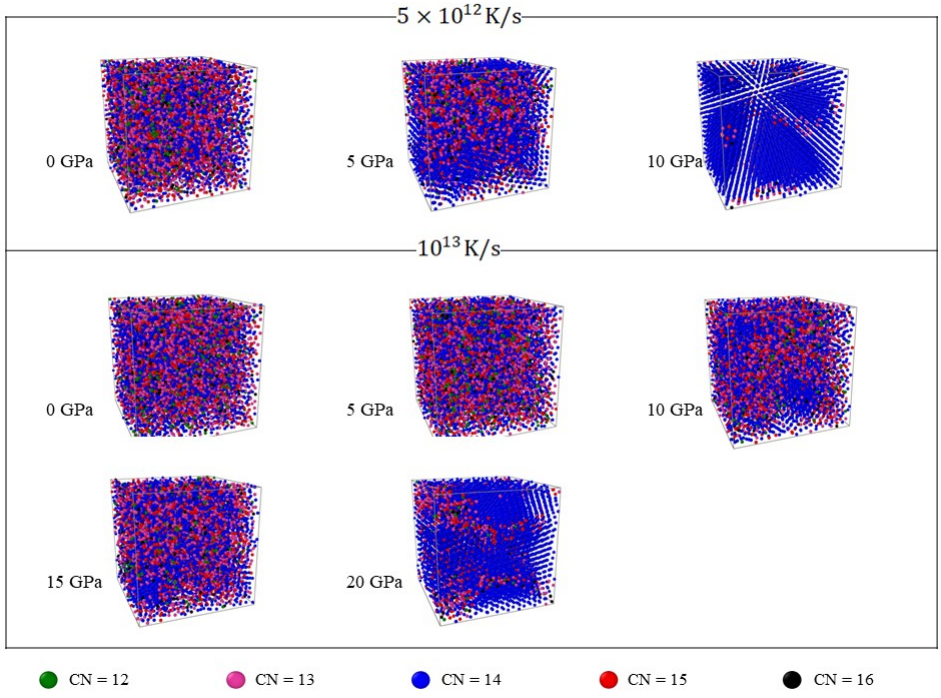

Figure 6: 3D visualization of Fe-MGs under two quenching conditions: cooling rate and pressure. The top snapshots represent 5×10^{12} for pressure from 0 to 10 GPa, and the bottom snapshots represent 1×10^{13} for pressure from 0 to 20 GPa, illustrating the different coordination numbers distributed in the Fe-MGs boxes.

hand, the effect of cooling rates on fragility is relatively weaker compared to pressure.

The impact of applied pressure extends beyond fragility, also affecting the relaxation temperature range. Higher pressures accelerate the attainment of the vitreous state by restricting atomic mobility and limiting relaxation processes. Remarkably, when pressure approaches vacuum conditions, the relaxation temperature becomes more influenced by the cooling rate, underscoring the significant role of cooling rate in the material's relaxation behavior.

The investigation of structural properties in Fe-MGs highlights the critical roles of pressure and cooling rate in determining atomic arrangement. Under increased pressure, short-range order strengthens, and crystal nucleation is promoted, resulting in a gradual rise in crystallinity. Notably, certain polyhedra, such as $< 0,4,4,6 >$ and $< 0,6,0,8 >$, exhibit significant percentage increases across

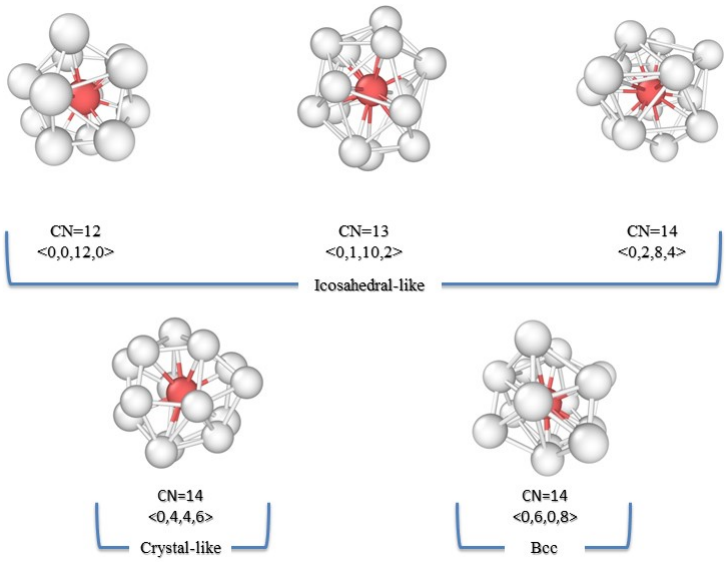

Figure 7: Snapshots illustrating configurations of the most abundant Voronoi polyhedra in the Fe system.

various quenching rates, underscoring their vital contributions to the structural evolution of metallic glass.

Furthermore, the correlation between pressure and density shows a predictable trend, with density increasing as pressure rises. On the other hand, an intriguing discovery emerges when examining the relationship between density and cooling rate. The data unequivocally demonstrates that density decreases with higher cooling rates, confirming the presence of free volume as a disorder within the glassy state. This observation is particularly pronounced after rapid cooling, as evidenced in Table 1 and Figure SM4.

The coordination number distribution in glass materials is influenced by pressure and cooling rate. Higher pressures result in a greater fraction of atoms with a coordination number of 14, indicating denser atomic packing. Conversely, rapid cooling rates lead to a broader distribution of coordination numbers beyond CN=14, suggesting a more disordered atomic arrangement (see Figure SM3). The average coordination number (ACN) increases with higher pressure, while the cooling rate has minimal impact on ACN, as shown in Table 1. Additionally, the interatomic distance between Fe atoms decreases from 2.47 Å to 2.41 Å with increasing pressure, and the cooling rate significantly affects this interatomic distance.

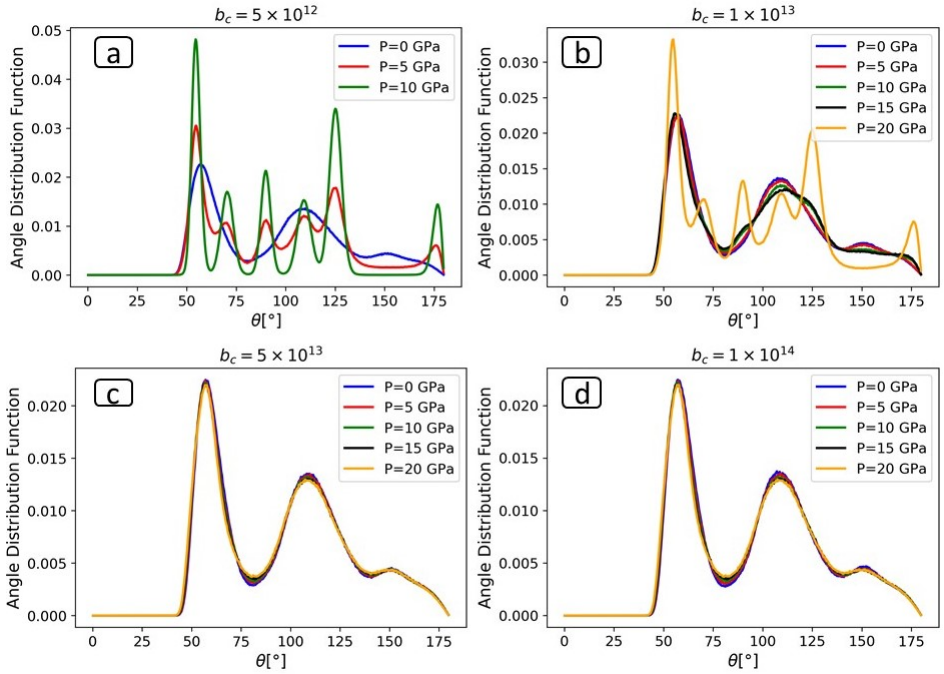

Figure 8: Angle Distribution Function (ADF) for Fe-Fe-Fe angles in Fe-MGs prepared at 300 K under various quenching conditions of pressure: (a) for the cooling rate of 5×10^{12} K/s, (b) for the cooling rate of 1×10^{13} K/s, (c) for the cooling rate of 5×10^{13} K/s, (d) for the cooling rate of 1×10^{14} K/s.

On the other hand, at a high cooling rate of 5×10^{13}, regardless of the value of pressure in the considered range (0 to 20 GPa), the angle distribution function shows almost two distinguishable peaks, one around 57.06° and the other around 111.06°, with a shoulder at 150.3° (Figure 8). In contrast, at a low cooling rate below 1×10^{13}, this behavior of two peaks and one shoulder is only evident at low pressure, while at 5×10^{12}, there are almost no such cases observed, unlike what is shown at high cooling rates.

These findings highlight the interplay between pressure applied during the glass transition process and cooling rate in shaping the fragility and atomic arrangement of Fe-MGs. Understanding these relationships is essential for tailoring the properties and performance of metallic glasses in various applications. Control over the cooling rate and applied pressure during the fabrication of metallic glasses could offer opportunities to optimize their properties for specific engineering applications. For instance, by adjusting the cooling rate, it might be possible

to achieve a desired balance between structural disorder and crystallinity, influencing mechanical properties, corrosion resistance, and other essential characteristics. Similarly, pressure-assisted processing could be explored to create Fe-MGs with tailored fragility and relaxation behavior for specific functional requirements.

5. Conclusion

This study investigated the effects of pressure and cooling rates on the kinetic and structural properties of iron metallic glasses (Fe-MGs) using molecular dynamics simulations with the embedded-atom potential (EAM). The main findings of this research can be summarized as follows:

- Pressure applied during the glass transition process also influenced T_g, with higher pressures leading to an elevated glass transition temperature. Pressure hindered atomic rearrangements necessary for the glass transition and increased the activation energy for atomic mobility.
- The fragility index (m) of Fe-MGs increased with pressure, indicating that higher pressure further impeded structural rearrangements and relaxation processes near T_g.
- Radial distribution function analysis revealed changes in local atomic arrangements with pressure and cooling rates, reflecting variations in atomic coordination and packing.
- Voronoi tessellation analysis showed that pressure promoted the stabilization and progressive nucleation of crystal-like clusters and body-centered cubic (bcc) structures, leading to more ordered atomic configurations and denser packing.
- The distribution of coordination numbers (CNs) highlighted a preference for a well-defined atomic arrangement with approximately 14 neighboring atoms under specific pressure-cooling rate combinations.
- The correlation between kinetic and structural results demonstrated the interplay between kinetic properties (activation energy, fragility index) and structural evolution (crystal-like clusters, bcc structures) in Fe-MGs.

These findings provide valuable insights into the behavior of Fe-MGs under varying thermodynamic conditions and offer a comprehensive understanding of

the fundamental mechanisms governing their glass transition and microstructural evolution. The observed correlations between kinetic and structural properties can be utilized to design and fabricate metallic glasses with tailored properties for specific applications. Additionally, the results presented here contribute to the existing knowledge in the field of metallic glasses and lay the foundation for future research and experiments in this area.

6. Acknowledgements

The authors would like to extend their gratitude for the generous provision of high-power computing resources by CALMIP, which enabled the completion of this research.

7. Declaration of Competing Interest

The authors declare that there are no conflicts of interest, including personal relationships or financial considerations, that could have influenced the publication of the study presented in this paper.

8. Supplementary Material

In this study, we provide additional figures to further illustrate the investigations conducted.

References

[1] W. Klement, R. Willens, P. Duwez, Non-crystalline structure in solidified gold–silicon alloys, Nature 187 (4740) (1960) 869–870.

[2] I. Donald, H. Davies, Prediction of glass-forming ability for metallic systems, Journal of Non-Crystalline Solids 30 (1) (1978) 77–85.

[3] A. Inoue, B. Shen, N. Nishiyama, Development and applications of late transition metal bulk metallic glasses, Bulk metallic glasses (2008) 1–25.

[4] M. Ashby, A. L. Greer, Metallic glasses as structural materials, Scripta Materialia 54 (3) (2006) 321–326.

[5] A. Inoue, B. L. Shen, A new fe-based bulk glassy alloy with outstanding mechanical properties, Advanced Materials 16 (23-24) (2004) 2189–2192.

[6] H. Li, Z. Lu, S. Wang, Y. Wu, Z. Lu, Fe-based bulk metallic glasses: Glass formation, fabrication, properties and applications, Progress in Materials Science 103 (2019) 235–318.

[7] C. Zhang, X.-m. Li, S.-Q. Liu, H. Liu, L.-J. Yu, L. Liu, 3d printing of zr-based bulk metallic glasses and components for potential biomedical applications, Journal of Alloys and Compounds 790 (2019) 963–973.

[8] C. Suryanarayana, A. Inoue, Bulk metallic glasses, CRC press, 2017.

[9] C. Suryanarayana, A. Inoue, Glass-forming ability of alloys, Bulk Metallic Glasses, CRC Press, Boca Raton, FL (2011) 49.

[10] H. Jabraoui, E. Achhal, A. Hasnaoui, J.-L. Garden, Y. Vaills, S. Ouaskit, Molecular dynamics simulation of thermodynamic and structural properties of silicate glass: Effect of the alkali oxide modifiers, Journal of Non-Crystalline Solids 448 (2016) 16–26.

[11] H. Jabraoui, Y. Vaills, A. Hasnaoui, M. Badawi, S. Ouaskit, Effect of sodium oxide modifier on structural and elastic properties of silicate glass, The Journal of Physical Chemistry B 120 (51) (2016) 13193–13205.

[12] J. Lu, G. Ravichandran, Pressure-dependent flow behavior of zr41. 2ti13. 8cu12. 5ni10be22. 5 bulk metallic glass, Journal of materials research 18 (9) (2003) 2039–2049.

[13] S. Mishra, S. Pal, Variation of glass transition temperature of al90sm10 metallic glass under pressurized cooling, Journal of Non-Crystalline Solids 500 (2018) 249–259.

[14] T. El hafi, O. Bajjou, H. Jabraoui, J. Louafi, M. Mazroui, Y. Lachtioui, et al., Effects of cooling rate on the glass formation process and the microstructural evolution of silver mono-component metallic glass, Chemical Physics 569 (2023) 111873.

[15] Y. Lachtioui, M. Kbirou, K. Saadouni, M. Sajieddine, M. Mazroui, Glass formation and structure evolution in the rapidly solidified monatomic metallic liquid pt under high pressure, Chemical Physics 538 (2020) 110805.

[16] S. Sengul, M. Celtek, U. Domekeli, Molecular dynamics simulations of glass formation and atomic structures in zr60cu20fe20 ternary bulk metallic alloy, Vacuum 136 (2017) 20–27.

[17] Q. Yu, X. Wang, H. Lou, Q. Cao, J. Jiang, Atomic packing in fe-based metallic glasses, Acta Materialia 102 (2016) 116–124.

[18] H. Jabraoui, A. Esteve, M. Schoenitz, E. L. Dreizin, C. Rossi, Atomic scale insights into the first reaction stages prior to al/cuo nanothermite ignition: influence of porosity, ACS applied materials & interfaces 14 (25) (2022) 29451–29461.

[19] H. Jabraoui, M. Badawi, S. Lebègue, Y. Vaills, Elastic and structural properties of low silica calcium aluminosilicate glasses from molecular dynamics simulations, Journal of Non-Crystalline Solids 499 (2018) 142–152.

[20] H. Jabraoui, S. Gin, T. Charpentier, R. Pollet, J.-M. Delaye, Leaching and reactivity at the sodium aluminosilicate glass−water interface: Insights from a reaxff molecular dynamics study, The Journal of Physical Chemistry C (2021). doi:DOI: 10.1021/acs.jpcc.1c07266.

[21] H. Jabraoui, A. Estève, S. Hong, C. Rossi, Initial stage of titanium oxidation in ti/cuo thermites: a molecular dynamics study using reaxff forcefields, Physical Chemistry Chemical Physics 25 (16) (2023) 11268–11277.

[22] H. Jabraoui, T. Charpentier, S. Gin, J.-M. Delaye, R. Pollet, Behaviors of sodium and calcium ions at the borosilicate glass–water interface: Gaining new insights through an ab initio molecular dynamics study, The Journal of Chemical Physics 156 (13) (2022) 134501.

[23] C.-W. Kim, H.-S. Yoo, J.-Y. Jeon, J.-I. Cho, S.-K. Hong, The effect of fe addition on microstructure, mechanical properties and electric conductivity of the as-cast al–mg–si alloys, Journal of Nanoscience and Nanotechnology 21 (3) (2021) 1915–1919.

[24] J. Ren, Y. Li, X. Liang, H. Kato, W. Zhang, Role of fe substitution for co on thermal stability and glass-forming ability of soft magnetic co-based co-fe-bpc metallic glasses, Intermetallics 147 (2022) 107598.

[25] A. P. Thompson, H. M. Aktulga, R. Berger, D. S. Bolintineanu, W. M. Brown, P. S. Crozier, P. J. in 't Veld, A. Kohlmeyer, S. G. Moore, T. D. Nguyen, R. Shan, M. J. Stevens, J. Tranchida, C. Trott, S. J. Plimpton, LAMMPS - a flexible simulation tool for particle-based materials modeling at the atomic, meso, and continuum scales, Comp. Phys. Comm. 271 (2022) 108171. doi:10.1016/j.cpc.2021.108171.

[26] X. W. Zhou, M. E. Foster, R. B. Sills, An fe-ni-cr embedded atom method potential for austenitic and ferritic systems, Journal of computational chemistry 39 (29) (2018) 2420–2431.

[27] A. Stukowski, Visualization and analysis of atomistic simulation data with ovito–the open visualization tool, Modelling and Simulation in Materials Science and Engineering 18 (1) (2009) 015012.

[28] D. Kilymis, J.-M. Delaye, S. Ispas, Behavior of sodium borosilicate glasses under compression using molecular dynamics, The Journal of Chemical Physics 143 (9) (2015) 094503.

[29] H. Jin, X. Gu, P. Wen, L. Wang, K. Lu, Pressure effect on the structural relaxation and glass transition in metallic glasses, Acta materialia 51 (20) (2003) 6219–6231.

[30] V. Brazhkin, Investigation of the crystallization of liquid iron under pressure: extrapolation of the melt viscosity into the megabar range, Journal of Experimental and Theoretical Physics Letters 68 (1998) 502–508.

[31] H. N. Ritland, Density phenomena in the transformation range of a borosilicate crown glass, Journal of the American Ceramic Society 37 (8) (1954) 370–377.

[32] D. J. Plazek, K. L. Ngai, Correlation of polymer segmental chain dynamics with temperature-dependent time-scale shifts, Macromolecules 24 (5) (1991) 1222–1224.

[33] R. Böhmer, C. A. Angell, Correlations of the nonexponentiality and state dependence of mechanical relaxations with bond connectivity in ge-as-se supercooled liquids, Physical Review B 45 (17) (1992) 10091.

[34] H. Jabraoui, S. Ouaskit, J. Richard, J.-L. Garden, Determination of the entropy production during glass transition: Theory and experiment, Journal of Non-Crystalline Solids 533 (2020) 119907.

[35] H. Jabraoui, M. Malki, A. Hasnaoui, M. Badawi, S. Ouaskit, S. Lebègue, Y. Vaills, Thermodynamic and structural properties of binary calcium silicate glasses: insights from molecular dynamics, Physical Chemistry Chemical Physics 19 (29) (2017) 19083–19093.

[36] M. Scott, The crystallization kinetics of fe-ni based metallic glasses, Journal of Materials Science 13 (1978) 291–296.

[37] C. T. Moynihan, Correlation between the width of the glass transition region and the temperature dependence of the viscosity of high-tg glasses, Journal of the American Ceramic Society 76 (5) (1993) 1081–1087.

[38] K. Ito, C. T. Moynihan, C. A. Angell, Thermodynamic determination of fragility in liquids and a fragile-to-strong liquid transition in water, Nature 398 (6727) (1999) 492–495.

[39] Y.-C. Hu, P.-F. Guan, Q. Wang, Y. Yang, H.-Y. Bai, W.-H. Wang, Pressure effects on structure and dynamics of metallic glass-forming liquid, The Journal of Chemical Physics 146 (2) (2017).

[40] H. Shintani, H. Tanaka, Universal link between the boson peak and transverse phonons in glass, Nature materials 7 (11) (2008) 870–877.

[41] R. Casalini, C. Roland, Scaling of the supercooled dynamics and its relation to the pressure dependences of the dynamic crossover and the fragility of glass formers, Physical Review B 71 (1) (2005) 014210.

[42] M. Paluch, J. Gapinski, A. Patkowski, E. W. Fischer, Does fragility depend on pressure? a dynamic light scattering study of a fragile glass-former, The Journal of Chemical Physics 114 (18) (2001) 8048–8055.

[43] L.-M. Wang, Z. Li, Z. Chen, Y. Zhao, R. Liu, Y. Tian, Glass transition in binary eutectic systems: Best glass-forming composition, The Journal of Physical Chemistry B 114 (37) (2010) 12080–12084.

[44] R. Busch, W. Liu, W. Johnson, Thermodynamics and kinetics of the mg 65 cu 25 y 10 bulk metallic glass forming liquid, Journal of Applied Physics 83 (8) (1998) 4134–4141.

[45] H. Gong, M. Sun, Z. Li, R. Liu, Y. Tian, L.-M. Wang, Kinetic fragility of binary and ternary glass forming liquid mixtures, The European Physical Journal E 34 (2011) 1–6.

[46] L.-M. Wang, C. A. Angell, R. Richert, Fragility and thermodynamics in nonpolymeric glass-forming liquids, The Journal of chemical physics 125 (7) (2006).

[47] R. Liu, D. Qi, S. Wang, Subpeaks of structure factors for rapidly quenched metals, Physical Review B 45 (1) (1992) 451.

[48] J. Finney, Random packings and the structure of simple liquids. i. the geometry of random close packing, Proceedings of the Royal Society of London. A. Mathematical and Physical Sciences 319 (1539) (1970) 479–493.

[49] P. Gaskell, A new structural model for transition metal–metalloid glasses, Nature 276 (5687) (1978) 484–485.

[50] J. Hwang, Nanometer scale atomic structure of zirconium based bulk metallic glass, Ph.D. thesis (2011).